Optofluidic Dye Lasers Based on Holey Fibers: Modeling and Performance Analysis

Zeeshan Rashid , *Student Member, OSA*, Alexandr Jonáš , *Member, OSA*,
Ryszard Buczyński, and Alper Kiraz , *Member, OSA*

Abstract—Holey optical fibers with air-filled openings can be turned into unconventional optofluidic components by selectively introducing a suitable liquid into their internal holes. Enhanced interaction between the light guided by the fiber and molecular species suspended in the confined liquid then forms the basis for designing unique optofluidic devices—filters, sensors, or lasers—whose operating characteristics are extremely sensitive to minute changes in the liquid composition. We present a comprehensive mathematical analysis of dye lasers based on suspended-core and hollow-core fibers, with aqueous solution of Rhodamine B dye injected into the internal holes of the fibers acting as the gain medium. Our model consists of coupled first-order differential equations that characterize the population of lasing levels and the variation of pump and signal laser powers along the fiber length in the steady state. We obtain optimum operating conditions of the proposed holey fiber dye lasers, such as the optimum fiber length and dye concentration, and compare their performance to conventional dye jet lasers. We conclude that the fiber variant of dye laser using the hollow-core fiber is superior in terms of low lasing threshold and high slope efficiency. The presented theoretical framework can find applications in designing practical holey fiber dye lasers serving as fiber-based alternatives of conventional dye jet lasers as well as novel biological/chemical sensors and bio-lasers.

Index Terms—Dye lasers, optical fiber lasers, optical fiber losses, optical fibers, optical pumping, scattering.

I. INTRODUCTION

OPTOFLUIDICS synergistically merges technological advances in photonics and microfluidics, enabling numerous novel applications that range from the fabrication of photonic devices controlled through liquid actuation and mixing (e.g. optofluidic lenses [1] or tunable optical resonators [2]) to the development of technologies for renewable energy production and storage [3]. A major strand of current optofluidics research is directed towards devising unconventional sources of laser light that utilize liquids as their fundamental structural element. The most prominent representatives of this class of photonic devices are biolasers that exploit biomolecules or living cells suspended in an aqueous buffer as their gain medium [4], [5]. Enhanced interaction of light with fluorescent biological particles located either directly inside the laser cavity or in its evanescent-field region enables building highly sensitive biochemical sensors [6], [7]. Moreover, specific self-recognition and self-assembly of biological molecules can be used for programmable modulation and switching of lasing action [8]. Other recent applications of optofluidic lasers include the development of compact tunable sources of coherent light [9], [10], temperature sensors [11], and flow rate sensors [12].

Typically, cavities of optofluidic lasers are integrated into specially designed microfluidic chips. The cavity itself can be based either on a miniaturized version of the standard Fabry-Perot etalon [13], [14] or it can employ distributed feedback mechanism [10], [15]. Another strategy makes use of whispering gallery mode (WGM) resonators formed by a thin-wall capillary; here, the resonant mode resides in the capillary wall and the gain medium located inside the capillary is coupled to the mode field evanescently [8]. Alternatively, solid materials can be avoided altogether with self-assembled all-liquid WGM cavities based on spherical liquid droplets that contain the gain medium dissolved in the droplet liquid [5]. While all these schemes work well for miniaturized analytical and sensing applications that require only picomoles of the gain medium and operate with laser emission powers in the range of microwatts [6], they cannot be readily scaled up in order to build high-power optofluidic lasers capable of delivering watts of coherent optical power. Therefore, an alternative cavity design is needed for implementing such lasers.

Holey fibers (also known as photonic crystal fibers or microstructured fibers) represent the most recent addition to the family of fiber-based optical waveguides. Generally characterized by the presence of carefully arranged arrays of air holes in their cross-section, holey fibers can be fabricated with parameters that are impossible to achieve in standard optical fibers, such as endlessly single-mode light guiding, large mode area, high numerical aperture (NA $\approx$ 0.9), and high damage threshold [16], [17]. Air-filled openings in holey fibers that run along the whole length of the fiber can also serve as microfluidic channels compatible with a wide range of fluids. Such a combination
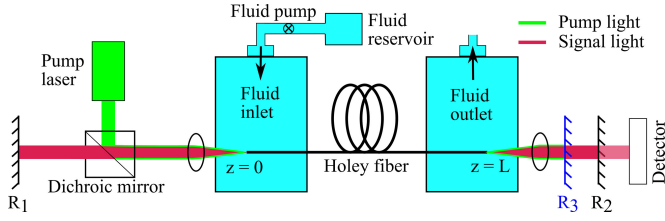
Fig. 1. Schematic diagram of a model optofluidic dye laser based on a holey fiber of total length L filled with an aqueous dye solution circulating through the fiber. Fabry-Perot-type laser cavity is formed between the input mirror (reflectivity R_1) and the output mirror (reflectivity R_2). The optofluidic laser is pumped by an external laser source coupled to the system using a dichroic mirror. Pumping efficiency is further increased with a pump mirror (reflectivity R_3) that reflects the pump light back into the fiber while transmitting the signal light.

of light guiding and fluid confinement in a single optofluidic element [18] has been recently exploited to achieve sensing of temperature, pressure, electric/magnetic field [19] and refractive index [20]. Furthermore, by selectively injecting a fluorophore-containing solution into the vacant space, the fiber can be turned into an effective housing for the gain medium of an optofluidic laser that is then formed by placing the liquid-filled fiber inside an external optical cavity (see Fig. 1 for illustration). With a proper design, the liquid-filled fiber can retain its light-guiding properties, ensuring an optimal overlap between the gain medium and the propagating pump and signal modes over a long distance along the fiber. Thus, optofluidic lasers based on holey fibers can potentially deliver high output powers, far exceeding $1-5$ W typically achieved by conventional dye jet lasers [21]. Similarly to the conventional fiber lasers, fiber geometry with large surface-to-volume ratio is advantageous for good thermal management critical in high-power applications [22]. These favorable properties make optofluidic fiber dye lasers an attractive alternative to conventional dye jet lasers, in which the dye solution circulates through a flow cell or propagates through open space in the form of a liquid jet stream. Because of their ability to generate monochromatic light over a broad range of visible wavelengths, tunable dye lasers have been a subject of intense research since their introduction in the early 1970s and have found numerous applications in medicine and spectroscopy [21], [23], [24].

Schematic diagram of a possible implementation of our model dye laser based on a holey fiber is shown in Fig. 1. A similar experimental configuration has been used previously in gas-laser experiments reported in [25]. The dye solution encapsulated within the fiber is continuously injected by a fluid pump so that the intracavity concentration of the dye is not affected by photobleaching; at the same time, the dye is optically pumped with external laser light coupled into and guided along the same fiber. Continuous wave (CW) pumping conditions are assumed in this paper. The gain medium can either directly overlap with the guided mode field for maximum excitation or it can couple to the evanescent tails of the mode for maximum propagation distance along the fiber. In general, the useful laser output power depends on the reflectivity R_2 of the cavity output mirror (see Fig. 1), which, therefore, has to be carefully optimized. In fiber-based lasers, abundant gain medium is efficiently excited and, thus, the internal power can reach high levels even for low

values of R_2. A realistic experimental system will suffer from additional losses due to imperfect coupling of light between the cavity and the fiber. These coupling losses can be estimated and included in the simulations by modifying the effective values of R_1 and R_2. Besides, designing of optimum optofluidic couplers that ensure efficient coupling of both light and liquid flow in and out of the holey fiber is a very critical challenge for the success of the holey fiber dye lasers studied in this manuscript [26], [27]. Recently, various experimental demonstrations of pulsed dye lasers [28]–[30], and pulsed [25] and CW [31] gas lasers that employ holey fibers have been reported.

The purpose of this paper is to carry out a comprehensive performance analysis of optofluidic fiber dye lasers, using rate equations that describe the excited-state population of the gain medium and the spatial variation of the pump and signal powers in the steady state of laser operation. We consider three different geometries of holey fiber dye lasers: double-cladding suspended-core fiber (SCF), double-cladding hollow-core fiber (HCF), and single-cladding HCF. We study the performance of holey fiber dye lasers for different concentrations of dye molecules and scattering loss coefficients. We demonstrate that holey fiber dye lasers operate most efficiently at an optimum fiber length; this is true even in the absence of scattering losses in the system. For benchmarking purposes, we also discuss the performance of dye jet lasers. Our analysis reveals that the performance of SCF-based dye lasers is considerably worse than all other cases due to very small coupling between the gain medium and the lasing mode. In contrast, double-cladding HCF-based dye lasers reach performance levels comparable to dye jet lasers, while single-cladding HCF-based dye lasers reach performance levels superior to all other cases.

The paper is organized as follows. In Section II, we define the cross-sectional geometries of both types of fibers (SCF and HCF). We also carry out electromagnetic simulations based on Finite Element Method (FEM) to determine the transverse profile of the guided modes of the fibers and calculate the effective mode field areas and filling factors. In Section III, we introduce the rate equation model of fiber dye lasers that is then applied to calculate the population of the upper lasing level and the distribution of the forward- and backward-propagating pump and signal powers. Subsequently, we determine the optimum fiber length at a given dye concentration and scattering loss coefficient, the threshold pump power, and the slope efficiency of the lasers. Section IV deals with the modeling of dye jet lasers using the same dye parameters as those considered for fiber dye lasers; in this section, we also compare the performance of the two laser systems. Finally, conclusions are drawn in Section V.

II. GEOMETRY OF HOLEY FIBERS AND CHARACTERIZATION OF THEIR GUIDED MODES

In the double-cladding SCF and double-cladding HCF geometries, we assume the inner cladding confines the lasing mode propagating in the suspended or hollow signal core whereas the outer air cladding formed by a ring of air holes confines the pump light in the multimode pump core [see Figs. 2(a) and 3(a)]. In comparison with the standard single-cladding approach, this
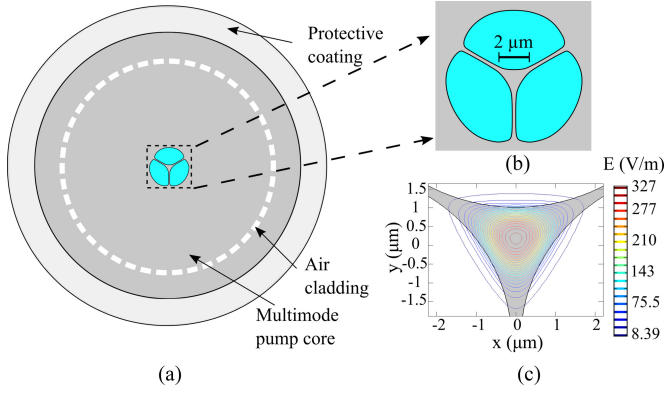
Fig. 2. Suspended-core fiber for optofluidic dye lasers. (a) Double-cladding SCF geometry. (b) Magnified view of the hole region filled with dye solution (blue color). (c) Distribution of the electric field amplitude $|E(x, y)|$ of the fundamental guided mode at 560 nm. Fiber design parameters: $A^{liquid} = 8.80 \times 10^{-7}$ cm^2.
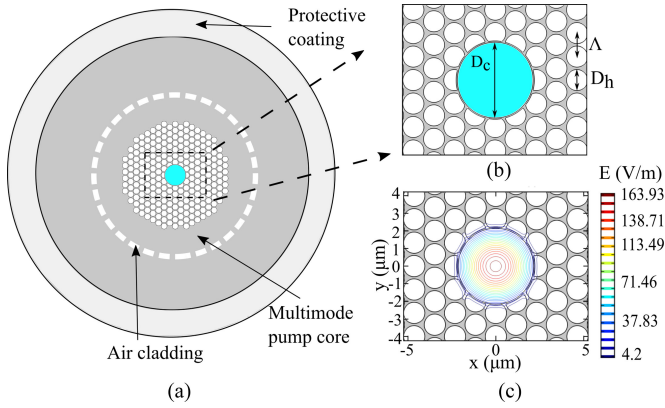

Fig. 3. Hollow-core fiber for optofluidic dye lasers. (a) Double-cladding HCF geometry. (b) Magnified view of the central hole filled with dye solution (blue color). (c) Distribution of the electric field amplitude $|E(x, y)|$ of the fundamental guided mode at 560 nm. Fiber design parameters: $D_c = 4.7\,\mu$m, $D_h = 1.2\,\mu$m, $D_h/\Lambda = 0.9$.

geometry provides a higher numerical aperture for coupling the pump light into the fiber (input NA ranging from 0.72 to 0.91), better thermal management, and lower pump losses [32]. As a third geometry, we consider single-cladding HCF, in which the pump beam is assumed to be fully coupled to the signal core that also confines the lasing mode. For the SCF design, the configuration used by Schartner *et al.* [33] operating at 532 nm is assumed (Fig. 2). Laser gain medium formed by Rhodamine B dye dissolved in water fills the fiber holes surrounding the suspended core, indicated by blue color. Since the refractive index of the aqueous dye solution ($n_{cl} = 1.33$) is smaller than that of the suspended silica fiber core ($n_c = 1.45$), the fiber infiltrated with the dye solution retains its light-guiding capacity. HCF geometry shown in Fig. 3 is inspired by a commercially available photonic crystal fiber [34]. The fiber is operated as a liquid-core light guide, with the central core opening infiltrated with aqueous dye solution and inner cladding holes filled with air ($n_{air} = 1$; see Fig. 3(b) for details) [35]. Consequently, a fiber that guides light due to the effective refractive index mechanism is obtained; the light is strongly confined within the central

hole filled with aqueous dye solution by total internal reflection for all visible wavelengths. The only difference between the double-cladding and single-cladding HCF geometry is the presence or absence of the outer air cladding in the fiber cross-section.

We used FEM to calculate the distributions of the electric and magnetic fields of fundamental guided modes in holey fibers at the signal (lasing) wavelength, $\lambda_s = 560$ nm. Transverse profiles of the electric field amplitude, $|E(x, y)|$, are shown in Figs. 2(c) and 3(c) for SCF and HCF, respectively. Knowing the transverse profile of the guided-mode fields, signal filling factor, Γ_s, can be calculated as the ratio of the signal power contained within the liquid-filled region, P_s^{liquid}, to the total power, P_s^{total}, of the guided signal mode as [36]:

$$\Gamma_s = \frac{\int_{liquid}(E_x H_y - E_y H_x)dxdy}{\int_{total}(E_x H_y - E_y H_x)dxdy}. \tag{1}$$

Here, E_x, E_y (H_x, H_y) represent the position-dependent transverse components of the electric (magnetic) field of the guided signal mode. The pump filling factor, Γ_p, is considered to be 1 for the case of single-cladding HCF. For the double-cladding SCF and double-cladding HCF cases, assuming the pump light intensity is uniform within the multimode pump core, Γ_p is given by the ratio of the cross-sectional area of liquid-filled region, A^{liquid}, marked by blue color in Figs. 2(a) and 3(a) to the total cross-sectional area of the multimode pump core, A^{total} ($\Gamma_p = A^{liquid}/A^{total}$). For a fair comparison, Γ_p is assumed to have the same value of 0.02 for both studied double-cladding cases.

III. MODELING OF HOLEY FIBER DYE LASERS

The following system of nonlinear, coupled differential equations was employed in modeling the operation of holey fiber dye lasers [37], [38]:

$$\frac{N_2(z)}{N} = \frac{\frac{P_p^{tot}(z)\Gamma_p \lambda_p \sigma_{ap}}{A_p} + \frac{P_s^{tot}(z)\Gamma_s \lambda_s \sigma_{as}}{A_s}}{\frac{hc}{\tau} + \frac{P_p^{tot}(z)\Gamma_p \lambda_p \sigma_p^{tot}}{A_p} + \frac{P_s^{tot}(z)\Gamma_s \lambda_s \sigma_s^{tot}}{A_s}}, \tag{2}$$

$$\pm\frac{dP_p^{\pm}(z)}{dz} = \Gamma_p \left[\sigma_p^{tot} N_2(z) - \sigma_{ap} N\right] P_p^{\pm}(z) - \alpha_p P_p^{\pm}(z), \tag{3}$$

$$\pm\frac{dP_s^{\pm}(z)}{dz} = \Gamma_s \left[\sigma_s^{tot} N_2(z) - \sigma_{as} N\right] P_s^{\pm}(z) - \alpha_s P_s^{\pm}(z). \tag{4}$$

In these equations, $N_2(z)$ is the population density of the upper lasing level, $P_p(z)$ and $P_s(z)$ represent the pump and signal powers as a function of distance z measured along the fiber, and the superscripts " $+$ " and " $-$ " correspond to the forward- and backward-propagating pump and signal powers, respectively. $P_{p(s)}^{tot}(z) = \left(P_{p(s)}^{+}(z) + P_{p(s)}^{-}(z)\right)$ denotes the sum of the forward- and backward-propagating pump (signal) powers, $\sigma_{p(s)}^{tot} = \left(\sigma_{ap(as)} + \sigma_{ep(es)}\right)$ is the sum of the absorption and stimulated emission cross-sections at the pump (signal) wavelength, $\alpha_p(\alpha_s)$ is the scattering loss coefficient at the pump (signal) wavelength, τ is the fluorescence lifetime of the excited

TABLE I
DESCRIPTIONS AND NUMERICAL VALUES OF PARAMETERS
USED IN THE RATE EQUATION MODEL [37], [38]

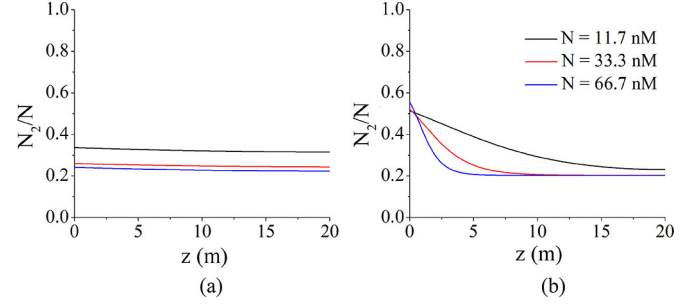| Param.	Description	Num. value
λ_p	Pump wavelength	532 nm
λ_s	Signal wavelength	560 nm
σ_{ap}	Absorption cross section at λ_p	3.42×10^{-16} cm^2
σ_{as}	Absorption cross section at λ_s	1.00×10^{-16} cm^2
σ_{ep}	Stimulated emission cross section at λ_p [40]	2.00×10^{-17} cm^2
σ_{es}	Stimulated emission cross section at λ_s	3.78×10^{-16} cm^2
α_p	Scattering loss coefficient at λ_p	2×10^{-4} cm^{-1}
α_s	Scattering loss coefficient at λ_s	2×10^{-4} cm^{-1}
$A_{p,\text{SCF}}$	Area of pump overlap with liquid in SCF	8.80×10^{-7} cm^2
$A_{s,\text{SCF}}$	Area of signal overlap with liquid in SCF	8.18×10^{-9} cm^2
$A_{p,\text{HCF}}$	Area of pump overlap with liquid in HCF	1.73×10^{-7} cm^2
$A_{s,\text{HCF}}$	Area of signal overlap with liquid in HCF	1.73×10^{-7} cm^2
τ	Fluorescence lifetime	4 ns
$\Gamma_{s,\text{SCF}}$	Signal filling factor for SCF	0.0143
$\Gamma_{s,\text{HCF}}$	Signal filling factor for HCF	0.9957
n_c	Refractive index of silica	1.45
n_{cl}	Refractive index of aqueous dye solution	1.33
R_1	Reflectivity of input mirror	0.99
R_2	Reflectivity of output mirror	0.50
R_3	Reflectivity of pump mirror	0.99
h	Planck's constant	6.63×10^{-34} J.s
c	Speed of light	3.00×10^8 m/s

Fig. 4. Normalized population of the upper lasing level, $N_2(z)/N$, at different N in (a) double-cladding and (b) single-cladding HCF dye lasers.

state, N is the uniform concentration of the gain medium, and $A_{p(s)}$ is the effective overlap area of the pump (signal) beam with the liquid gain medium. Since the pump light is assumed to be uniform across the multimode pump core, $A_p = A^{liquid}$. The same definition of A_p is also adopted for the single-cladding HCF. A_s is calculated using the concept of effective mode area as [39]:

$$A_s = \frac{\left(\int\int_{liquid} |E(x,y)|^2 dxdy \right)^2}{\int\int_{liquid} |E(x,y)|^4 dxdy} . \tag{5}$$

In Eq. (5), integration is carried out over the liquid-filled cross-sectional area. Values of all parameters that appear in our calculations are listed in Table I; some of them are material constants while the remaining ones are calculated by FEM simulations described in the previous section. Taking the pump power coupled into the fiber at $z = 0$ to be P_{in}, the solution of the coupled differential equations (2) – (4) is carried out subject to four boundary conditions: $P_p^+(0) = P_{in}$, $P_p^-(L) = R_3 P_p^+(L)$, $P_s^+(0) = R_1 P_s^-(0)$ and $P_s^-(L) = R_2 P_s^+(L)$, where L is the total length of the fiber. When solving the coupled differential equations (2)–(4), $P_p^-(0)$ and $P_s^-(0)$ are initially guessed using the shooting method [38]. Subsequently, the guessed values are adjusted by the nonlinear solver after several iterations to satisfy the boundary conditions at $z = L$ for both pump and signal powers. In all calculations, R_1 and R_3 are considered to be 0.99, while R_2 is considered to be 0.50 except for the results presented in Fig. 10, where R_2 is a variable.

In the following, we carry out detailed numerical analysis of the different geometries of holey fiber dye lasers introduced in Section II. Among these geometries, double-cladding SCF layout is observed to perform considerably worse than both double-cladding HCF and single-cladding HCF layouts in terms of optic threshold pump power and slope efficiency. Therefore, the initial analysis is performed only for the double-

cladding and single-cladding HCF geometries, and the double-cladding SCF geometry is discussed only briefly at the end of Section III. In order to ensure the studied laser systems operate above the threshold, we chose P_{in} to be $1\,W$ for the double-cladding and single-cladding HCF laser calculations and $25\,W$ for the double-cladding SCF laser calculations. In all calculations, the value of α_p was kept constant at 2×10^{-4} cm^{-1}.

A. Spatial Variations of Upper Lasing Level Population

For typical laser systems based on rare-earth-doped fibers, $\sigma_{as} << \sigma_{es}$ and $\sigma_{as} << \sigma_{ap}$. This results in the second term in the numerator of Eq. (2) being negligible with respect to the first term, leading to a very small value of $N_2(z)/N$ everywhere along the fiber [38]. In contrast, for a dye-based gain medium, σ_{as} is of the same order as σ_{es} and σ_{ap} (for Rhodamine B, $\sigma_{es} \approx 3.78\sigma_{as}$ and $\sigma_{ap} \approx 3.42\sigma_{as}$). Higher absorption at the signal wavelength then results in $N_2(z)$ being of the same order of magnitude as N, which leads to larger values of $N_2(z)/N$. In Fig. 4, we show the evolution of $N_2(z)/N$ along the fiber length calculated for double-cladding HCF [part (a)] and single-cladding HCF [part (b)] for different values of N, assuming $\alpha_s = 2 \times 10^{-4}$ cm^{-1} and the total fiber length $L = 20$ m. It is notable that, in the single-cladding HCF, the relative population of the upper lasing level $N_2(z)/N$, varies significantly with z, in contrast to the double-cladding HCF layout. This behavior results from highly efficient absorption of pump light by the gain medium in the single-cladding HCF geometry with $\Gamma_p = 1$; the gain medium is strongly pumped near the beginning of the fiber and pumping efficiency then falls off rapidly, as the pump beam is progressively absorbed by the dye molecules.

B. Spatial Variations of Pump and Signal Powers

Variation of the pump power $P_p^{\pm}(z)$ with distance z along the fiber is governed by Eq. (3). Since losses dominate the change in $P_p^{\pm}(z)$, both $P_p^+(z)$ and $P_p^-(z)$ decay along their respective directions of propagation. The profiles of $P_p^+(z)$ and $P_p^-(z)$ for three different values of N and $\alpha_s = 2 \times 10^{-4}$ cm^{-1} are plotted in Fig. 5 for both double-cladding [part (a)] and single-cladding [part (b)] HCF. For the double-cladding HCF, $P_p^+(z)$ does not decay to 0 at $z = L$ due to a low Γ_p. On the other hand, for the single-cladding HCF with $N > 11.7$ nM and the total fiber length $L = 20$ m, $P_p^+(z)$ decays virtually to 0 at $z = L$, as the
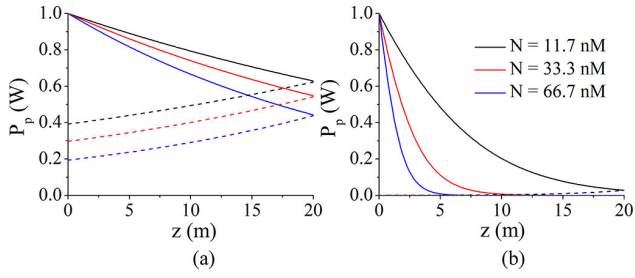
Fig. 5. $P_p^+(z)$ (——) and $P_p^-(z)$ (- - -) at different N in (a) double-cladding and (b) single-cladding HCF dye lasers.
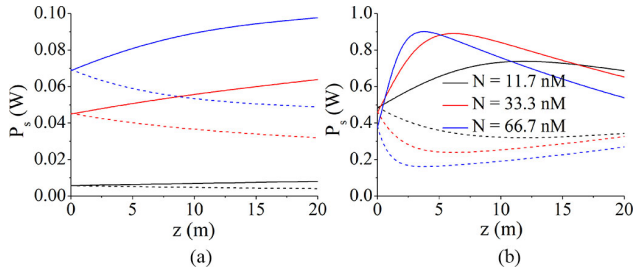

Fig. 6. $P_s^+(z)$ (——) and $P_s^-(z)$ (- - -) at different N in (a) double-cladding and (b) single-cladding HCF dye lasers, assuming $\alpha_s = 2 \times 10^{-4}$ cm^{-1}.

Fig. 7. $P_s^+(z)$ (——) and $P_s^-(z)$ (- - -) at different α_s in (a) double-cladding and (b) single-cladding HCF dye lasers, assuming $N = 33.3$ nM.

Fig. 8. Variation of L_{opt} (- - -) and $P_{out}(L_{opt})$ (——) with N at different α_s in (a) double-cladding and (b) single-cladding HCF dye laser.

pump beam is efficiently absorbed ($\Gamma_p = 1$). Hence, the power $P_p^-(z)$ of backward-propagating pump light can be neglected and the pump reflector R_3 (see Fig. 1) is effectively redundant in the system. However, when N and/or L are lowered, reflector R_3 becomes important for efficient pumping of the gain medium.

Eq. (4) describes the variation of the signal power $P_s^\pm(z)$ with distance z along the fiber. Within the initial section of the fiber where $N_2(z)$ reaches its highest values (see Fig. 4), stimulated emission dominates over absorption and scattering losses under proper parametric conditions and, consequently, $P_s^+(z)$ is gradually amplified. At the point $z = z_{max}$ where the gain is exactly equal to the sum of absorption and scattering losses, $P_s^+(z)$ reaches a maximum. Since $N_2(z)$ is monotonically decreasing with z, for $z > z_{max}$, losses become dominant, leading to a gradual decrease of $P_s^+(z)$. In general, this trend is observed even in the absence of scattering losses (i.e. for $\alpha_s = 0$). Hence, there is always an optimum fiber length, $L_{opt} = z_{max}$, at which $P_s^+(z)$ is maximum. At this optimum length, maximum output power can be obtained from the holey fiber dye laser. For a cavity with an output coupler of reflectivity R_2, this maximum output power can be expressed as: $P_{out}(L_{opt}) = P_s^+(L_{opt})[1 - R_2]$. Spatial profiles of $P_s^+(z)$ and $P_s^-(z)$ are plotted for three different values of N assuming $\alpha_s = 2 \times 10^{-4}$ cm^{-1} in Fig. 6. The rate of change of $P_s^+(z)$ with z depends directly on the variations of $N_2(z)$. Since $N_2(z)$ falls off more rapidly for larger N for both fiber types (see Fig. 4), maximum of $P_s^+(z)$ shifts to a smaller value of z_{max} and $P_s^+(z)$ increases and decays faster. According to Eq. (4), the dynamics of spatial changes of $P_s^\pm(z)$ is also determined by scattering losses. The distributions of $P_s^+(z)$ and $P_s^-(z)$ along the fiber length at $N = 33.3$ nM and three different values of α_s are shown in Fig. 7. Clearly, an increase in α_s leads to an overall decrease in the value of $P_s^\pm(z)$ due to larger losses within the laser cavity. At the same time,
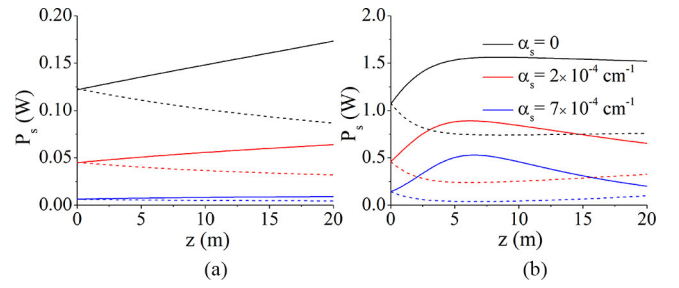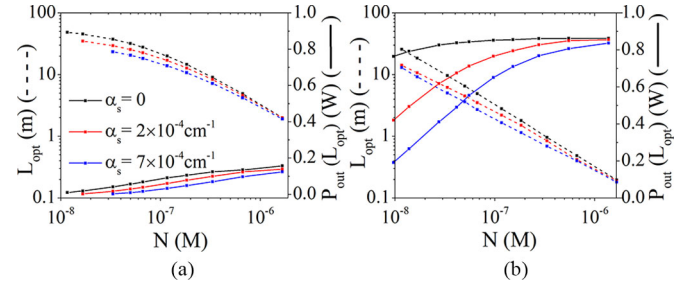
with higher scattering losses, $P_s^+(z)$ reaches its maximum at lower values of z; thus, L_{opt} is also reduced.

The optimum fiber length, L_{opt}, is determined by an interplay between the dye concentration, scattering losses, and pump power. Due to the nonlinear nature of the system, L_{opt} is a variable that changes when the fiber length L is changed. In order to determine the value of L_{opt}, at which the fiber-dye laser provides the highest possible signal power, we iteratively solved Eqs. (2)–(4) for different values of L and considered the value of L_{opt} that maximized the peak of the spatial profile of P_s^+. The variation of L_{opt} with N at different values of α_s is plotted in Figs. 8(a) and 8(b) for double-cladding and single-cladding HCF dye lasers, respectively. Due to less efficient absorption of the pump light in the double-cladding HCF geometry with smaller Γ_p, double-cladding HCF lasers display values of L_{opt} that are consistently higher than those of single-cladding HCF lasers for all values of N. For a given HCF geometry, higher absorption of the pump and signal light at higher N results in smaller L_{opt}. The total output power at the optimum fiber length $P_{out}(L_{opt})$ is also shown in Fig. 8 as a function of N for double-cladding and single-cladding HCF lasers. In general, it is observed that laser operation at higher N is preferable for achieving maximum output power. As the dye concentration increases above $\sim 1\,\mu$M, output power and optimum fiber length become relatively insensitive to small variations in α_s and the output power tends to saturate. Hence, good operating parameters for double-cladding HCF and single-cladding HCF are revealed as [$N \sim 1\,\mu$M, $L_{opt} \sim 1 - 10$ m] and [$N \sim 1\,\mu$M, $L_{opt} \sim 0.1 - 1$ m], respectively. We note that thermal and photobleaching effects are not included in our analysis. Both of these effects will generally result in changes in the optimum operating parameters of holey fiber dye lasers.
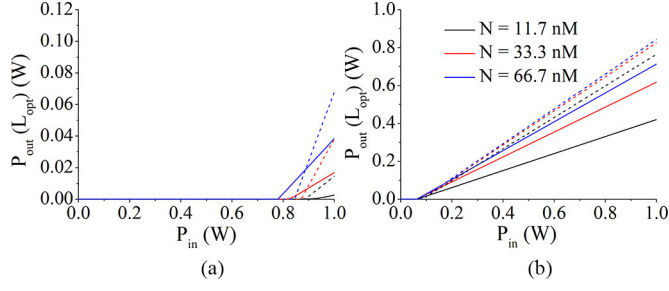
Fig. 9. Variation of $P_{out}(L_{opt})$ with P_{in} at different N for $\alpha_s = 0$ (- - -) and $\alpha_s = 2 \times 10^{-4}$ cm^{-1} (——) in (a) double-cladding and (b) single-cladding HCF dye laser.
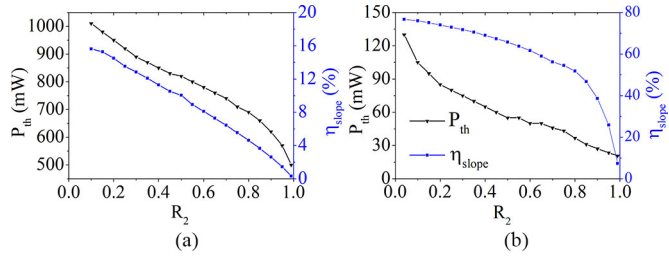

Fig. 10. Variation of P_{th} and η_{slope} with R_2 at $N = 33.3$ nM in (a) double-cladding and (b) single-cladding HCF dye laser.

Fig. 11. Variation of P_{th}, L_{opt} and η_{slope} with N for $\alpha_s = 0$ (- - - -) and $\alpha_s = 2 \times 10^{-4}$ cm^{-1} (——) in (a) double-cladding and (b) single-cladding HCF dye laser.

Fig. 12. (a) Variation of $P_{out}(L_{opt})$ with P_{in} at different N for $\alpha_s = 0$ (- - -) and $\alpha_s = 2 \time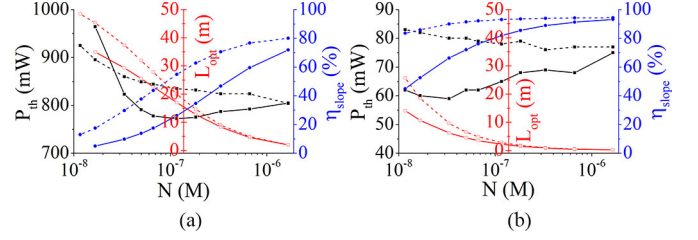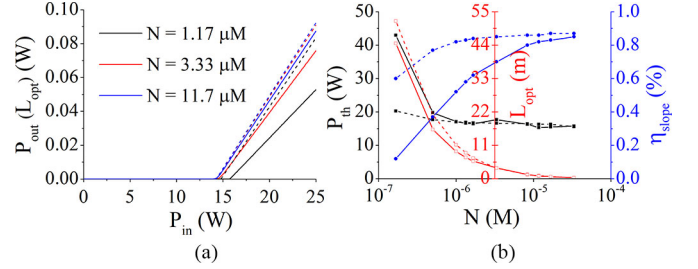s 10^{-4}$ cm^{-1} (——) in double-cladding SCF dye laser. (b) Variation of P_{th}, L_{opt} and η_{slope} with N for $\alpha_s = 0$ (- - - -) and $\alpha_s = 2 \times 10^{-4}$ cm^{-1} (——) in double-cladding SCF dye laser.

C. Threshold Pump Power and Slope Efficiency

In order to determine the slope efficiency, η_{slope}, and threshold pump power, P_{th}, of our holey fiber dye lasers, we solved the coupled rate equations (2)–(4) for increasing values of P_{in} and different values of R_2. Assuming that the system was always operated at optimum conditions, which were different for each studied P_{in} and R_2, we set the fiber length equal to L_{opt} and, subsequently, calculated the output power of the laser as $P_{out}(L_{opt})$. Exemplary plots showing $P_{out}(L_{opt})$ as a function of P_{in} for $R_2 = 0.50$ are shown in Fig. 9. From the dependence of $P_{out}(L_{opt})$ on P_{in}, both η_{slope} and P_{th} can be directly determined. Figure 10 shows the change in η_{slope} and P_{th} with R_2 for both double-cladding and single-cladding HCF lasers. For both geometries, η_{slope} and P_{th} are observed to decrease monotonically with R_2. Hence, the trade-off between low P_{th} and high η_{slope} is clearly visible, and R_2 value should be carefully selected for the required operating regime.

D. Optofluidic Fiber Dye Laser Summary

P_{th}, L_{opt}, and η_{slope} are the key characteristics of the holey fiber dye lasers studied in this paper. The values of these characteristic parameters as a function of N are summarized in Figs. 11(a), 11(b), and 12(b) for the double-cladding HCF, single-cladding HCF, and double-cladding SCF geometries, respectively. In these figures, we consider both zero ($\alpha_s = 0$; dashed lines) and non-zero ($\alpha_s = 2 \times 10^{-4}$ cm^{-1}; solid lines) signal scattering losses. For the double-cladding SCF, the value of P_{th} is larger than ~ 15 W and η_{slope} remains below 1% for all studied N and α_s. This results from the very small values of Γ_p and Γ_s that characterize this geometry and cause inefficient

pumping of the gain medium and inefficient coupling of the dye emission to the guided lasing mode. Hence, we conclude that the considered double-cladding SCF geometry performs significantly worse than the other two holey fiber dye laser geometries. Out of these two geometries, single-cladding HCF dye laser performs better than the double-cladding HCF dye laser in all aspects. With the single-cladding HCF geometry, P_{th} and η_{slope} values of ~ 80 mW and $> 90\%$, respectively, can be simultaneously achieved for $L_{opt} \sim 0.2$ m and $N \sim 1\,\mu$M. On the other hand, double-cladding HCF dye laser reaches P_{th} and η_{slope} values of ~ 800 mW and $> 60\%$ for $L_{opt} \sim 5$ m and $N \sim 1\,\mu$M. As it is shown in the following section, these are still quite respectable performance parameters when dye jet lasers are considered. It is notable that, for some configurations of fiber dye lasers studied in Fig. 11, the value of P_{th} for $\alpha_s = 0$ is higher than P_{th} of a laser with finite scattering losses and the same value of N. This seemingly counterintuitive result is due to different values of L_{opt} that are obtained for different α_s with the optimization procedure described in Sec. III-B. In general, smaller α_s is associated with a larger L_{opt}, which in turn requires a higher pump power for creating threshold population inversion along the fiber length.

IV. MODELING OF CONVENTIONAL DYE JET LASERS

Dye jet lasers involve continuous flow of a dye solution through a narrow nozzle forming a jet of liquid gain medium. This liquid jet then passes through the common focal point of the pump and signal laser beams with the focal-point diameters ω_{p0}, ω_{s0}, respectively [41]. Pike developed analytical expressions for calculating the threshold pump power and the slope
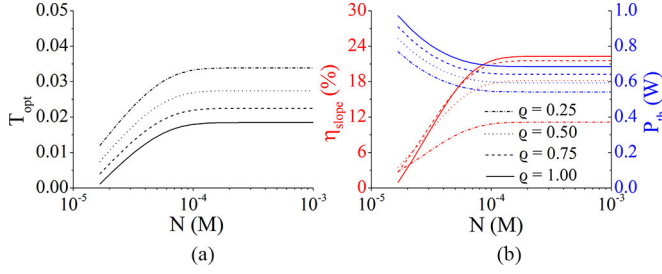
Fig. 13. Dye jet laser characteristics as a function of N for different values of ϱ. (a) T_{opt}. (b) η_{slope} (left ordinate) and P_{th} (right ordinate).

efficiency of such dye jet lasers [42]. Within Pike's formalism, the threshold pump power P_{th} is given as:

$$P_{th} = (T + L_c)B, \qquad (6)$$

where T is the useful single-pass loss of the cavity due to the output coupler transmission $[T = (-\ln R_2)/2]$, L_c is the non-useful single-pass loss of the cavity related to absorption and scattering, and $B = [(1 + \varrho)b_p hc]/[4\sigma_{as}\tau(1 - e^{-N\sigma_{ap}d})]$. In the expression for B, ϱ is the beam diameter ratio (also known as the mode match parameter) defined as $\varrho = \omega_{p0}^2/\omega_{s0}^2$, d is the length of the path traversed by the pump and signal laser beams within the gain medium, and b_p is the confocal parameter (or depth of focus) of the pump beam which is equal to the distance between the two end points of the Rayleigh range, i.e $b_p = 2z_{R,p} = (2\pi\omega_{p0}^2)/\lambda_p$. The output signal power can then be expressed as [43]:

$$P_{out} = \frac{TA(P_{in} - P_{th})}{T + L_c}, \qquad (7)$$

where $A = [(1 - e^{-N\sigma_{ap}d})\varrho]/\sqrt{1 + \varrho^2}$.

The maximum output power that is available from the laser at a given pump power, P_{in}, is obtained at the optimum value of useful cavity losses, T_{opt}, that maximizes Eq. (7). The resultant T_{opt} and η_{slope} at T_{opt} are given as:

$$T_{opt} = L_c \left(\sqrt{\frac{P_{in}}{BL_c}} - 1 \right), \qquad (8)$$

$$\eta_{slope} = \frac{dP_{out}}{dP_{in}} = \frac{AT_{opt}}{T_{opt} + L_c}. \qquad (9)$$

In dye jet lasers, T_{opt} is a parameter analogous to L_{opt} in fiber dye lasers and it characterizes the system performance. Using the parameters of Rhodamine B dye listed in Table I and assuming optimum transmission $T = T_{opt}$ of the output coupler at each studied configuration, we calculated P_{th} and η_{slope} for typical operating parameters of a dye jet laser ($d = 0.2$ cm, $\omega_{po} = 20\,\mu$m, $L_c = 4\%$) [44]. Concentration dependences of T_{opt}, P_{th}, and η_{slope} are plotted in Fig. 13 for different values of ϱ. In calculating the values presented in Fig. 13, T_{opt} was determined at each N and ϱ using Eq. (8) and assuming $P_{in} = 1$ W, which represents typical pumping conditions above threshold. Subsequently, P_{th}, and η_{slope} were found from Eqs. (6) and (9), respectively.

For small values of N, the absolute population inversion and, consequently, the optical gain at a given signal intensity

is low [41]. The steady-state operation of the laser requires corresponding lowering of the overall losses of the cavity. Thus, for optimal performance, the reflectivity of the output coupler has to be increased, resulting in smaller T_{opt}. Smaller T_{opt} also leads to a smaller η_{slope}, as dictated by Eq. (9). When N is increased, P_{th} decreases and η_{slope} increases in accordance with Eqs. (6) and (9), respectively. For the dye concentration varying from $20\,\mu$M to 1 mM, P_{th} is observed to change between 1 W and 541 mW for different values of ϱ. This range of P_{th} of a typical dye jet laser is significantly better than that of the double-cladding SCF laser (15.3–43 W), comparable to that of the double-cladding HCF laser (772 – 964 mW), and significantly worse than that of the single-cladding HCF laser (59–83 mW). Maximal η_{slope} calculated for the dye jet laser is 22%. This value is much higher than the maximum calculated for the SCF laser ($\eta_{slope} = 0.9\%$), but significantly lower than the maximal efficiencies of both double-cladding and single-cladding HCF lasers ($\eta_{slope} = 80\%$ and $\eta_{slope} = 94\%$, respectively). From Fig. 13, it is evident that saturation is observed in both P_{th} and η_{slope} beyond $N \simeq 0.12$ mM. Thus, from the practical point of view, it is not advantageous to operate dye jet lasers too high above this saturation concentration.

V. CONCLUSION

In this paper, we have introduced optofluidic dye lasers based on holey fibers and investigated their potential for complementing or replacing dye jet lasers in high-power applications. We have developed a mathematical model of such fiber laser systems using coupled steady-state rate equations and solved these equations to determine the laser performance characteristics under various operating conditions. In our parametric study, we have considered three different fiber laser geometries with different mode areas and pump/signal filling factors, in particular, double-cladding SCF laser, double-cladding HCF laser, and single-cladding HCF laser. For benchmarking purposes, we have also compared our results with the performance characteristics of dye jet lasers. From our analysis, we can draw the following main conclusions:

- Among the studied fiber dye laser geometries and the dye jet laser, the single-cladding HCF laser has been found to perform the best in terms of low P_{th} and high η_{slope}. This is mainly due to the large pump and signal filling factors in this arrangement that allow for efficient collection and transport of light within the active gain medium. Double-cladding HCF laser has been found to perform comparably to the dye jet laser when the pump filling factor is similar to or larger than the value of $\Gamma_p = 0.02$ assumed in the paper.
- Taking into account better thermal management and ease of coupling of the pump beam into the fiber, double-cladding HCF laser has the potential to be the most practical geometry for holey fiber dye lasers.
- Double-cladding SCF geometry has been found to be highly inefficient, with $P_{th} > 10$ W and $\eta_{slope} < 1\%$, caused mostly by the extremely small value of Γ_s that results from evanescent coupling of the signal light to the guided mode of the fiber.

- For a given dye concentration, N, there is an optimum fiber length, L_{opt}, that maximizes the output power of the holey fiber dye laser. Our analysis shows that good operating parameters for double-cladding and single-cladding HCF lasers are $N \sim 1\,\mu$M, $L_{opt} \sim 4.7$ m and $N \sim 1\,\mu$M, $L_{opt} \sim 0.45$ m, respectively. We note that thermal effects and dye photobleaching can impose additional limitations on the determination of the best-performance values of N and L_{opt}.

In conclusion, detailed analysis carried out in this paper shows the suitability of single-cladding and double-cladding HCF geometries for holey fiber dye laser applications. Optimum operating conditions of the proposed optofluidic lasers have been determined considering realistic parameters. Practical holey fiber dye lasers that can serve as fiber-based alternatives of conventional dye jet lasers as well as novel biological/chemical sensors and bio-lasers can be designed using the presented framework. Natural extension of our work will incorporate thermal effects and dye photobleaching into the analysis of laser performance. This way, holey fiber dimensions including the fiber length and the cross-section of the liquid-filled channel can be further optimized and optimal flow speed of the dye solution through the fiber can be determined.

REFERENCES

[1] P. Fei *et al.*, "Discretely tunable optofluidic compound microlenses," *Lab Chip*, vol. 11, no. 17, pp. 2835–2841, Jun. 2011.

[2] U. Levy, K. Campbell, and A. Groisman, "On-chip microfluidic tuning of an optical microring resonator," *Appl. Phys. Lett.*, vol. 88, no. 11, pp. 1111071–1111073, Jan. 2006.

[3] D. Erickson, D. Sinton, and D. Psaltis, "Optofluidics for energy applications," *Nature Photon.*, vol. 5, pp. 583–590, Sep. 2011.

[4] M. C. Gather and S. H. Yun, "Single-cell biological lasers," *Nature Photon.*, vol. 5, pp. 406–410, Sep. 2011.

[5] A. Jonáš *et al.*, "*In vitro* and *in vivo* biolasing of fluorescent proteins suspended in liquid microdroplet cavities," *Lab Chip*, vol. 14, no. 16, pp. 3093–3100, Aug. 2014.

[6] X. Fan and I. M. White, "Optofluidic microsystems for chemical and biological analysis," *Nature Photon.*, vol. 5, pp. 591–597, Sep. 2011.

[7] X. Fan and S. H. Yun, "The potential of optofluidic biolasers," *Nature Methods*, vol. 11, no. 2, pp. 141–147, Jan. 2014.

[8] Q. Chen *et al.*, "Self-assembled DNA tetrahedral optofluidic lasers with precise and tunable gain control," *Lab Chip*, vol. 13, no. 17, pp. 3351–3354, Jun. 2013.

[9] W. Song, A. E. Vasdekis, and D. Psaltis, "Elastomer based tunable optofluidic devices," *Lab Chip*, vol. 12, no. 19, pp. 3590–3597, Jun. 2012.

[10] A. Bakal *et al.*, "Tunable on chip optofluidic laser," *Appl. Phys. Lett.*, vol. 107, no. 21, Nov. 2015, Art. no. 211105.

[11] F. Lahoz *et al.*, "A compact and portable optofluidic device for detection of liquid properties and label-free sensing," *J. Phys. D, Appl. Phys.*, vol. 50, no. 21, May 2017, Art. no. 215103.

[12] Y. Gong *et al.*, "Sensitive optofluidic flow rate sensor based on laser heating and microring resonator," *Microfluid Nanofluid*, vol. 19, no. 6, pp. 1497–1505, Oct. 2015.

[13] D. V. Vezenov *et al.*, "A low-threshold, high-efficiency microfluidic waveguide laser," *J. Amer. Chem. Soc.*, vol. 127, no. 25, pp. 8952–8953, Jun. 2005.

[14] G. Aubry *et al.*, "A multicolor microfluidic droplet dye laser with single mode emission," *Appl. Phys. Lett.*, vol. 98, no. 11, Mar. 2011, Art. no. 111111.

[15] Z. Li *et al.*, "Single mode optofluidic distributed feedback dye laser," *Opt. Express*, vol. 14, no. 2, pp. 696–701, Jan. 2006.

[16] J. Broeng *et al.*, "Photonic crystal fibers: A new class of optical waveguides," *Opt. Fiber Technol.*, vol. 5, no. 3, pp. 305–330, Jul. 1999.

[17] P. S. Russell, "Photonic-crystal fibers," *J. Lightw. Technol.*, vol. 24, no. 12, pp. 4729–4749, Dec. 2006.

[18] A. Sudirman and W. Margulis, "All-fiber optofluidic component to combine light and fluid," *IEEE Photon. Technol. Lett.*, vol. 26, no. 10, pp. 1031–1033, May 2014.

[19] S. Ertman, P. Lesiak, and T. R. Wolinski, "Optofluidic photonic crystal fiber-based sensors," *J. Lightw. Technol.*, vol. 35, no. 16, pp. 3399–3405, Aug. 2017.

[20] B. Shuai *et al.*, "A multicore holey fiber based plasmonic sensor with large detection range and high linearity," *Opt. Express*, vol. 20, no. 6, pp. 5974–5986, Mar. 2012.

[21] J. T. F. Johnston, R. H. Brady, and W. Proffitt, "Powerful single-frequency ring dye laser spanning the visible spectrum," *Appl. Opt.*, vol. 21, no. 13, pp. 2307–2316, Jul. 1982.

[22] D. Richardson *et al.*, "High power fiber lasers: Current status and future perspectives," *J. Opt. Soc. Amer. B*, vol. 27, no. 11, pp. B63–B92, Nov. 2010.

[23] O. G. Peterson, S. A. Tuccio, and B. B. Snavely, "CW operation of an organic dye solution laser," *Appl. Phys. Lett.*, vol. 17, no. 6, pp. 245–247, Oct. 1970.

[24] F. J. Duarte, *High Power Dye Lasers*, vol. 65, A. E. Siegman, Ed. Berlin, Germany: Springer-Verlag, 1991.

[25] A. V. V. Nampoothiri *et al.*, "Hollow-core optical fiber gas lasers (hofglas): A review [invited]," *Opt. Mater. Express*, vol. 2, no. 7, pp. 948–961, Jul. 2012.

[26] A. M. Cubillas *et al.*, "Photonic crystal fibres for chemical sensing and photochemistry," *Chem. Soc. Rev.*, vol. 42, no. 22, pp. 8629–8648, Apr. 2013.

[27] R. M. Gerosa *et al.*, "All-fiber high repetition rate microfluidic dye laser," *Optica*, vol. 2, no. 2, pp. 186–193, Feb. 2015.

[28] A. E. Vasdekis *et al.*, "Fluidic fibre dye lasers," *Opt. Express*, vol. 15, no. 7, pp. 3962–3967, Mar. 2007.

[29] Y. Yonenaga *et al.*, "Random laser of dye-injected holey photonic-crystal fiber," *Phys. Rev. A*, vol. 92, no. 1, Jul. 2015, Art. no. 013824.

[30] A. M. Stolyarov *et al.*, "Microfluidic directional emission control of an azimuthally polarized radial fibre laser," *Nature Photon.*, vol. 6, pp. 229–233, Mar. 2012.

[31] A. V. V. Nampoothiri *et al.*, "CW hollow-core optically pumped I2 fiber gas laser," *Opt. Lett.*, vol. 40, no. 4, pp. 605–608, Feb. 2015.

[32] M. Franczyk *et al.*, "Phosphate Yb^{3+} doped air-cladding photonic crystal fibers for laser applications," *Photon. Lett.*, vol. 6, no. 1, pp. 47–49, Mar. 2014.

[33] E. P. Schartner, H. E. Heidepriem, and T. M. Monro, "Low concentration fluorescence sensing in suspended-core fibers," *Proc. SPIE*, vol. 7753, pp. 77534Q1–77534Q4, May 2011.

[34] "NKT Photonics," Brochure. [Online]. Available: http://www.nktphotonics.com/wp-content/uploads/sites/3/2015/01/HC-532.pdf

[35] L. C. Van *et al.*, "Supercontinuum generation in photonic crystal fibres with core filled with toluene," *J. Opt.*, vol. 19, no. 12, pp. 1–9, Nov. 2017.

[36] M. Gong *et al.*, "Numerical modeling of transverse mode competition in strongly pumped multimode fiber lasers and amplifiers," *Opt. Express*, vol. 15, no. 6, pp. 3236–3246, Mar. 2007.

[37] M. Aas, Q. Chen, A. Joná, A. Kiraz, and X. Fan, "Optofluidic FRET lasers and their applications in novel photonic devices and biochemical sensing," *IEEE J. Sel. Topics Quantum Electron.*, vol. 22, no. 4, pp. 188–202, Aug. 2016.

[38] I. Kelson and A. Hardy, "Optimization of strongly pumped fiber lasers," *J. Lightw. Technol.*, vol. 17, no. 5, pp. 891–897, May 1999.

[39] G. P. Agarwal, *Nonlinear Fiber Optics*, 3rd ed. Amsterdam, The Netherlands: Elsevier, 2001.

[40] Y. Yamamoto and R. E. Slusher, *Optical Processes in Microcavities*, B. Elias and W. Claude, Eds. Boston, MA, USA: Springer, 1995.

[41] K. H. Drexhage *et al.*, *Dye Lasers*, 1st ed, F. P. Schafer, Ed. Heidelberg, Germany: Springer-Verlag, 1973.

[42] H. A. Pike, "Organic dye lasers," Ph.D. dissertation, Inst. Optics, Univ. Rochester, Rochester, NY, USA, 1971.

[43] H. W. Schroder *et al.*, "A high-power single-mode CW dye ring laser," *Appl. Phys.*, vol. 14, no. 4, pp. 377–380, Dec. 1977.

[44] D. Frolich *et al.*, "Efficient frequency doubling of CW dye laser radiation," *Appl. Phys.*, vol. 11, no. 1, pp. 97–101, Sep. 1976.

Zeeshan Rashid received the B.S. and M.S. degrees from the University of Engineering and Technology, Lahore, Pakistan, in 2007 and 2012, respectively. Currently, he is working toward the Ph.D. degree in electrical and electronics engineering in Koç University, Istanbul, Turkey. Between 2008 and 2014, he was a Lecturer with the Islamia University of Bahawalpur, Bahawalpur, Pakistan. His research interests include modeling of fiber lasers, microfabrication of surface assisted liquid manipulation systems, preparation of chemically reconfigurable surfaces using plasma/light, and microdroplet manipulation for cell sorting and drug discovery.

Alexandr Jonáš received the M.S. degree in biophysics from Masaryk University, Brno, Czech Republic, in 1996, and the Ph.D. degree in physical and materials engineering from The Brno University of Technology, Brno, Czech Republic, in 2001. He was a post-doc with the European Molecular Biology Laboratory, Germany, and The University of Texas at Austin, USA, and held research and academic positions with the Czech Academy of Sciences, Institute of Scientific Instruments, Brno, Czech Republic, Koç University, Turkey, and Istanbul Technical University, Turkey. Currently, he is a Research Scientist with the Institute of Scientific Instruments. His research interests include the development and applications of optical micro-manipulation, microscopy, and spectroscopy techniques for the study of living cells and individual biomolecules, the characterization of novel miniature optical components based on liquids, and the analysis of thermophysical properties of supercritical fluids and fluid mixtures.

Ryszard Buczyński received the M.S. and Ph.D. degrees in physics from the Warsaw University of Technology, Warsaw, Poland, in 1994 and 1999, respectively, and the Ph.D. degree in applied science from the Vrije Universiteit Brussel, Brussels, Belgium, in 2000. During his academic career, he held post-doc positions with Vrije Universiteit Brussel, Belgium, and Heriot-Watt University, U.K. Currently, he is an Associate Professor with the Institute of Electronic Materials Technology, Warsaw, Poland, and the Faculty of Physics with the University of Warsaw, Warsaw, Poland. He leads an interuniversity research team Microoptics and Photonic Crystal Fibers Group. His research interests include photonic crystal fibers, supercontinuum generation, microoptics, and microfluidics. Recently, his research focuses on the development of nonlinear photonic crystal fibers based on soft glasses and nanostructured microoptical components.

Alper Kiraz received the B.S. degree in electrical and electronics engineering from Bilkent University, Ankara, Turkey, in 1998, and the M.S. and Ph.D. degrees in electrical and computer engineering from the University of California, Santa Barbara, Santa Barbara, CA, USA, in 2000 and 2002, respectively. Between 2002 and 2004, he was a post-doc with the Institute for Physical Chemistry, Ludwig-Maximilians University, Germany. He joined Koç University in 2004 and became a Full Professor in 2014. Between 2014 and 2015, he was a Visiting Professor with the Biomedical Engineering Department, the University of Michigan, Ann Arbor, USA. His research team pursues projects targeting the development of novel optofluidic lab-on-a-chip devices, molecular and gas sensors, optofluidic-based renewable energy solutions, and confocal microscope device concepts.